FlyTera: Echo State Learning for Joint Access and Flight Control in THz-enabled Drone Networks

Sabarish Krishna Moorthy
Department of Electrical Engineering
University at Buffalo, SUNY
Buffalo, NY 14260
Email: sk382@buffalo.edu

Zhangyu Guan
Department of Electrical Engineering
University at Buffalo, SUNY
Buffalo, NY 14260
Email: guan@buffalo.edu

***Abstract*—Terahertz (THz)-band communications has been envisioned as a key technology to support ultra-high-data-rate applications in 5G-beyond (or 6G) wireless networks. Compared to the microwave and mmWave bands, the main challenges with the THz band are in its i) large path loss hence limited network coverage and ii) visible-light-like propagation characteristics hence poor support of mobility in blockage-rich environments. This paper studies quantitatively the applicability of THz-band communications in mobile blockage-rich environments, focusing on a new network scenario called *FlyTera*.**

In *FlyTera*, a set of hotspots mounted on flying drones collaboratively provide data streaming services to ground users, in the microwave, mmWave and THz bands. We first provide a mathematical formulation of *FlyTera*, where the objective is to maximize the network spectral efficiency by jointly controlling the flight of the drone hotspots, their association to the ground users, and the spectrum bands used by the users. To solve the resulting problem, which is shown to be a mixed integer nonlinear nonconvex programming (MINLP) problem, we design distributed solution algorithms based on a combination of echo state learning and reinforcement learning techniques. An extensive simulation campaign is then conducted with SimBAG, a newly developed Simulator of Broadband Aerial-Ground wireless networks. It is shown that no single spectrum band can meet the requirements of high data rate and wide coverage simultaneously. Moreover, from the network-level point of view, THz-band communications can significantly benefit from the mobility of the flying drones, and on average $4-6$ times *higher (rather than lower)* throughput can be achieved in mobile than in static environments.

***Index terms*—** Terahertz Band; Millimeter-wave Band; Mircowave Band; Wireless Drone Networks; Echo State Learning.

I. Introduction

Communications in the terahertz band (i.e., THz, with frequency ranging from 100 GHz to 10 THz) is a key technology to meet the increasing demands of bandwidth-hungry applications in 5G-beyond and the envisioned 6G wireless networks, e.g., wireless virtual/augmented reality [1]. Compared to lower frequency bands, e.g., sub-6 GHz and mmWave bands, there are two main challenges with the THz band. First, its communication range is significantly reduced because of the large signal attenuation in THz band in radio in-air environments. For example, the attenuation due to water vapor and oxygen absorption is approximately $0.6-1000$ dB/km for THz band, while it is 0.01 dB/km at sub-6 GHz band and $0.3-0.6$ dB/km for the mmWave band [2]. Second, the THz links can be easily blocked because of the visible-light-like directional waves in extremely high frequency range.

978-1-7281-1062-2/20/$31.00 2020 © IEEE

In the past few years, significant research efforts have been directed towards addressing these challenges, focusing on either THz or mmWave bands. For example, in [3], [4] Han et al. propose a multi-wideband waveform design for the THz band, which improves the communication distance by dynamical varying the rate and the transmit power on each sub-window. The concept of ultra-massive MIMO communications was studied in [5] to increase the communication distance and the achievable capacity of THz-band communications. In mobile environments, fast beam search and alignment schemes have been proposed in [6]–[9]. For example, Hassanieh et al. propose Agile-Link in [6], which can provably find the optimal direction in logarithmic number of measurements. BeamSpy is proposed in [8] to instantaneously predict the quality of mmWave beams without the costly beam searching. Readers are referred to [10], [11] and references therein for an excellent survey of the main results in this area.

Most of these above discussed work require to redesign the lower layers (i.e., physical and link) of the communicating devices' protocol stack, and hence are not backward compatible. Moreover, these work either focus on only single link or static networking scenarios, while the applicability of THz-band communications for mobile wireless networking has not been thoroughly explored so far.

Novelty and Contributions. This paper aims at understanding from a network perspective the applicability of THz-band communications and how it can complement the lower-frequency bands in mobile blockage-rich environments. Inspired by the newly emerging drone cells [12], in this paper we focus on a network scenario called *FlyTera*, where a set of hotspots mounted on flying drones collaboratively provide data streaming services to ground users in the microwave, mmWave and THz bands. We consider FlyTera because the drone hotspots can be deployed dynamically at network run time, and hence i) it is more likely for them to establish line-of-sight (LOS) links to their users in blockage-rich environments; and ii) the network coverage and spectral efficiency can be enhanced by dynamically deploying more drone hotspots in areas with higher user density and higher traffic demand.

There are two major challenges to address in FlyTera. First, it is challenging for the distributed drone hotspots to coordinate with each other to achieve extended network coverage while still maintaining high-data-rate wireless links. This is because a drone hotspot may fly away from the ground network infrastructure when it moves closer to the users, hence reducing the data rate of the backhaul link. Second, the spectrum access and association strategies of the ground users are closely coupled with the drone hotspot locations and the interference levels on each spectrum band. This makes it both essential yet challenging to achieve a good tradeoff between network coverage and network spectral efficiency. To the best of our knowledge, this is the first work studying the joint access and flight control by jointly considering the microwave, mmWave and THz bands in mobile blockage-rich environments.

We claim the following three main contributions:

- We first formulate mathematically the control problem in FlyTera, where the objective is to maximize the network-wide spectral efficiency by jointly determining the flight of the drone hotspots, their association to the ground users, and the spectrum bands used by the users. It is shown that the resulting problem is a mixed integer nonlinear non-convex programming (MINLP) problem.
- We design distributed algorithms to solve the MINLP problem based on a combination of the echo state learning and reinforcement learning techniques. The echo state learning is shown to be able to predict the optimal movements for the drone hotspots with nearly-constant, low computational complexity in dynamic network environments.
- We develop a new event-driven, universal broadband simulator called SimBAG for integrated aerial-ground wireless networking. An extensive simulation campaign has been conducted based on SimBAG, which proves the great potential of THz-band communications from a network point of view. Results indicate that significantly $(4-6$ times) *higher* throughput can be achieved by THz-band communications in mobile than in static networks.

The rest of the paper is organized as follows. In Section II, we discuss the related work. In Section III, we present the system model and problem formulation. The distributed algorithm design is described in Section IV, and in Section V we discuss the development of SimBAG and analyze the performance evaluation results. Finally, we draw the main conclusions in Section VI.

II. Related Work

Drone-assisted spectrum access has drawn significant research attention [13]–[22]. For example, in [13] Yang et al. propose prediction methods for path loss and delay spread in air-to-ground millimetre-wave channels based on machine learning. In [14], the authors propose a tractable three-dimensional (3D) spatial model for evaluating the average downlink performance of unmanned aerial vehicle (UAV) networks in the mmWave bands. Zhu et al. realize in [15] flexible coverage by exploring 3D beamforming for mmWave UAV communications with a phased uniform planar array. In [16], Gapeyenko et al. investigate the use of UAVs to mitigate the impact of blockage on the backhaul links. In [17], the authors propose a fast beam tracking scheme to achieve high-quality communications in the mmWave band. Xiao et al. explore in [18] the use of mmWave spatial-division multiple access to improve the cellular network capacity. In [19], the authors evaluate the performance of the UAV-assisted mmWave network in urban environments utilizing access points carried by UAVs. In [20], Feng et al. propose a spectrum management architecture and evaluate the performance of the proposed mmWave based wireless backhaul in UAV-assisted cellular networks. In [21], Chen et al. study the resource management for virtual reality (VR) appliations in UAV-enabled LTE over unlicensed (LTE-U) network. Please refer to [22] for an excellent survey of the main results in this area. Different from these work, in this paper we focus on a new network scenario called FlyTera, where drone hotspots and ground users are allowed to operate in the microwave, mmWave and THz bands, and study how different spectrum bands complement each other in mobile blockage-rich environments.

III. System Model and Problem Formulation

In FlyTera there are a set of ground and drone base stations collaboratively providing access services to ground users in the microwave band f^{mc}, mmWave band f^{mm}, and THz band f^{tz}. Define the set of spectrum bands $\mathcal{F}$ as $\mathcal{F} \triangleq \{f^{\mathrm{mc}}, f^{\mathrm{mm}}, f^{\mathrm{tz}}\}$. Denote $\mathcal{B}_{\mathrm{grd}}, \mathcal{B}_{\mathrm{fly}}$ and $\mathcal{U}$ as the sets of the ground base stations (GBS), flying drone base stations (FBS) and users, respectively. Let $\mathcal{B}$ represent the set of all the base stations and $\widetilde{\mathcal{B}}$ the set of all the nodes, i.e., $\mathcal{B} = \mathcal{B}_{\mathrm{grd}} \cup \mathcal{B}_{\mathrm{fly}}$ and $\widetilde{\mathcal{B}} = \mathcal{B} \cup \mathcal{U}$. Our objective is to, given the blockage distribution in the network area, maximize the network spectral efficiency by jointly controlling the flight of the FBSs, their association with the ground users, as well as the spectrum bands used by the users. Next we describe the blockage, link and spectrum access models sequentially.

A. Blockage Model

Let $\mathcal{K}$ represent the set of blockages in the network. As illustrated in Fig. 1, each blockage $k \in \mathcal{K}$ is represented as a

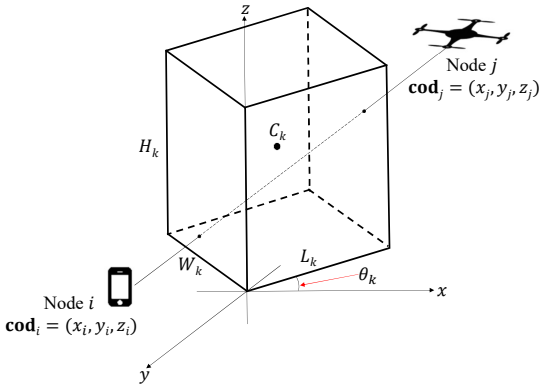

Fig. 1: Illustration of the blockage model in FlyTera.

rectangle of dimensions $L_k \times W_k \times H_k$, with L_k, W_k and H_k being the length, width and height of the blockage, respectively. Denote C_k as the center of blockage k. The orientation of blockage k, denoted as θ_k, is considered to be uniformly distributed in $[0,\ 2\pi]$. Define $\mathbf{P}_k^{\text{blk}}(C_k, L_k, W_k, H_k, \theta_k)$ as the set of points contained in blockage k.

Let $\mathbf{cod}_i = (x_i, y_i, z_i)$ denote the coordinate vector of node $i \in \widetilde{\mathcal{B}}$ (the phone in Fig. 1), with x_i, y_i and z_i being the x-, y- and z-axis components, respectively. Similarly, denote $\mathbf{cod}_j$ as the coordinate vector of node $j \in \widetilde{\mathcal{B}}$ (the drone in Fig. 1). Further define $\mathbf{P}_{ij}^{\text{seg}}$ as the point set of the segment connecting nodes i and j. Finally, use $\mathrm{I}(\mathbf{cod}_i, \mathbf{cod}_j, k)$ to indicate whether blockage k is blocking the link between nodes i and j, with $\mathrm{I}(\mathbf{cod}_i, \mathbf{cod}_j, k) = 1$ if yes, i.e., $\mathbf{P}_{ij}^{\text{seg}} \cap \mathbf{P}_k^{\text{blk}}(C_k, L_k, W_k, H_k, \theta_k) \neq \phi$, and $\mathrm{I}(\mathbf{cod}_i, \mathbf{cod}_j, k) = 0$ otherwise. Then, given the set $\mathcal{K}$ of blockages, the total number of blockages in the link between nodes i and j, denoted as $K^{i,j}$, can be expressed as

$$K^{i,j} = \sum_{k \in \mathcal{K}} \mathrm{I}(\mathbf{cod}_i, \mathbf{cod}_j, k),\ \forall i, j \in \widetilde{\mathcal{B}}. \tag{1}$$

B. Link Model

In this section we describe the interference model focusing on ground users in $\mathcal{U}$, while the model can be derived similarly for flying base stations in $\mathcal{B}_{\text{fly}}$. To this end, we first describe the path loss model.

Path Loss. Denote $L_{i,j}(f)$ as the path loss between nodes $i, j \in \widetilde{\mathcal{B}}$ operating in frequency band $f \in \mathcal{F}$. Then $L_{i,j}(f)$ can be modelled as in [23]

$$L_{i,j}(f) = \beta_0^{K_{i,j}} \left(\frac{4\pi f}{C}\right)^2 (d_{i,j})^{\alpha_{i,j}(f)} \tag{2}$$

where C is the speed of light, $\alpha_{i,j}(f)$ is the path-loss exponent for the link between nodes i and j in frequency band f, $K_{i,j}$ defined in (1) represents the number of blockages in the link, $\beta_0 \in [0,\ 1]$ is the per-blockage absorption coefficient [24] [25], and finally $d_{i,j} = d_{i,j}(\mathbf{cod}_i, \mathbf{cod}_j)$ denotes the distance between nodes i and j, i.e.,

$$d_{i,j} = \sqrt{(x_i - x_j)^2 + (y_i - y_j)^2 + (z_i - z_j)^2}, \tag{3}$$

given coordinate vectors $\mathbf{cod}_i$ and $\mathbf{cod}_j$ defined in Section III-A for nodes i and j, respectively.

Microwave-Band Link. Denote γ_u^{mc} as the SINR of ground user $u \in \mathcal{U}$ if it receives on the microwave frequency band f^{mc}, then γ_u^{mc} can be expressed as

$$\gamma_u^{\text{mc}} = \frac{P_{i(u)}^{\text{mc}} L_{i(u),u}(f^{\text{mc}})}{\sum\limits_{j \in \mathcal{B}^{\text{mc}}/i(u)} P_j^{\text{mc}} L_{j,u}(f^{\text{mc}}) + N_0^{\text{mc}}} \tag{4}$$

where $\mathcal{B}^{\text{mc}} \subset \mathcal{B}$ represents the set of BSs operating on this band, and $i(u) \in \mathcal{B}^{\text{mc}}$ represents the serving BS of user $u \in \mathcal{U}$; $P_{i(u)}^{\text{mc}}$ and P_j^{mc} are the transmission power of the serving BS $i(u)$ and interfering BS $j \in \mathcal{B}^{\text{mc}}/i(u)$, respectively; $L_{i(u),u}(f^{\text{mc}})$ and $L_{j,u}(f^{\text{mc}})$ are the path loss defined in (2), and finally N_0^{mc} is the power of noise at node u in the microwave band. Let $\mathcal{U}_{i(u)}^{\text{mc}} \in \mathcal{U}$ represent the set of users served by BS $i(u)$ in this band, and consider that its transmission time is shared among the users it serves based on time-division multiple access (TDMA). Then the rate achievable by user u in this band, denoted as $R_u(f^{\text{mc}})$, can be written as

$$R_u(f^{\text{mc}}) = \frac{B^{\text{mc}}}{|\mathcal{U}_{i(u)}^{\text{mc}}|} \log_2(1 + \gamma_u^{\text{mc}}), \tag{5}$$

where $|\cdot|$ represents the cardinality of a set, i.e., the number of users served by BS $i(u)$ in this frequency band for our case.

MmWave-Band Link. Let $P_{i(u)}^{\text{mm}}$ denote the transmission power of the serving base station of user u (i.e., $i(u)$) in the mmWave band. Further denote $\mathcal{U}_{i(u)}^{\text{mm}} \in \mathcal{U}$ as the set of users served by BS $i(u)$ and $|\mathcal{U}_{i(u)}^{\text{mm}}|$ as the number of users in $\mathcal{U}_{i(u)}^{\text{mm}}$. Different from the microwave band, where the BS serves its users based on TDMA, in mmWave band the BS is able to serve the users simultaneously with the directional mmWave-band links. Let $P_{i(u),u'}^{\text{mm}}$ represent the transmission power of BS $i(u)$ allocated to user $u' \in \mathcal{U}_{i(u)}^{\text{mm}}$, then we have

$$\sum_{v \in \mathcal{U}_{i(u)}^{\text{mm}}} P_{i(u),v}^{\text{mm}} \leq P_{i(u)}^{\text{mm}},\ \forall u \in \mathcal{U}^{\text{mm}}. \tag{6}$$

The received SINR of user $u \in \mathcal{U}$ in this band, denoted as γ_u^{mm}, can then be written as

$$\gamma_u^{\text{mm}} = \frac{P_{i(u),u}^{\text{mm}} L_{i(u),u}(f^{\text{mm}}) G_{\max}^{\text{mm}} \widetilde{G}_{\max}^{\text{mm}}}{\sum\limits_{u' \in \mathcal{U}^{\text{mm}}/u} P_{i(u'),u'}^{\text{mm}} L_{i(u'),u}(f^{\text{mm}}) G_{i(u'),u}^{\text{mm}} \widetilde{G}_{u,i(u')}^{\text{mm}} + N_0^{\text{mm}}} \tag{7}$$

where $\mathcal{U}^{\text{mm}}$ represents the set of all the users operating in the mmWave band, and N_0^{mm} is the power of noise in this band at each user. In (7), $L_{i(u),u}(f^{\text{mm}})$ represents the path loss between BS $i(u)$ and user u in the mmWave band; $G_{i(u'),u}^{\text{mm}}$ and $\widetilde{G}_{u,i(u')}^{\text{mm}}$ represent the transmit gain of BS $i(u')$ and receive gain of user u respectively; $G_{\max}^{\text{mm}}$ and $\widetilde{G}_{\max}^{\text{mm}}$ denote the maximum transmit gain of BSs and maximum receive gain of

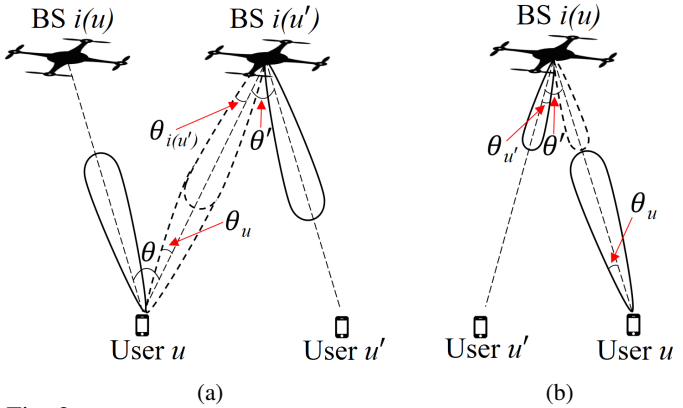

(a) (b)

Fig. 2: Interference model for the mmWave-band links: (a) inter-BS interference; (b) intra-BS interference.

users, respectively. Denote the resulting link rate as $R_u(f^{\rm mm})$ for user u, then we have

$$R_u(f^{\rm mm}) = B^{\rm mm}\log_2(1+\gamma_u^{\rm mm}), \tag{8}$$

where $B^{\rm mm}$ is the bandwidth of the mmWave frequency band.

We consider sectorized interference model as in [26] to determine the transmit and receive gains, i.e., $G^{\rm mm}_{i(u'),u}$ and $\widetilde{G}^{\rm mm}_{u,i(u')}$ in (7). As illustrated in Fig. 2, let $\theta \in [-\pi,\pi]$ denote the offset angle of the antenna boresight direction of user u with respect to the reference direction, and θ' as the offset angle for the drone base station. Here, the reference direction refers to the direction along which the transmitting and receiving beams are perfectly aligned, as indicated by the dashed beams in Fig. 2. Denote θ_u and $\theta_{i(u')}$ as the beamwidth of user u and BS $i(u')$, respectively. Then, the transmit gain for BS $i(u')$ and receive gain of user u can be determined as follows, taking Fig. 2(a) as an example:

$$G^{\rm mm}_{i(u'),u} = \begin{cases} G^{\rm mm}_{\max}, \text{ if } \theta' \le \theta_{i(u')} \\ G^{\rm mm}_{\min}, \text{ otherwise} \end{cases} \tag{9}$$

for the transmit gain, and

$$\widetilde{G}^{\rm mm}_{u,i(u')} = \begin{cases} G^{\rm mm}_{\max}, \text{ if } \theta \le \theta_u \\ G^{\rm mm}_{\min}, \text{ otherwise} \end{cases} \tag{10}$$

for the receive gain.

THz-Band Link. The SINR achievable by a user in the THz band can be derived similarly as in (7)-(10) for the mmWave band, except that only LOS transmissions will be considered because of the significantly higher path loss. Then, we have $K_{i,j}=0$ in (2) and the path loss can be rewritten as

$$L_{i,j}(f^{\rm tz}) = \left(\frac{4\pi f^{\rm tz}}{C}\right)^2 (d_{i,j})^{\alpha_{i,j}(f^{\rm tz})}, \tag{11}$$

where $d_{i,j}$ defined in (3) is the distance between nodes i and j, and $\alpha_{i,j}(f^{\rm tz})$ represents the path loss exponent in the THz band. Denote the resulting SINR as $\gamma_u^{\rm tz}$ for user u and the corresponding link rate as $R_u(f^{\rm tz})$.

C. Spectrum Access Model

Consider single-band spectrum access for the ground users and multi-band spectrum access for the base stations, i.e., each user is allowed to use at most one frequency band at the same time, while each base station is able to serve multiple users in different frequency bands. Then we have

$$\sum_{f\in\mathcal{F}} \psi(u,f) \le 1,\ \forall u \in \mathcal{U} \tag{12}$$

where $\psi(u,f)$ is the frequency selection function, with $\psi(u,f)=1$ if frequency band f is used by user u, and $\psi(u,f)=0$ otherwise. Then the overall access link rate of user $u\in\mathcal{U}$, denoted as $R_u^{\rm ac}$, can be expressed as

$$R_u^{\rm ac} = \sum_{f\in\mathcal{F}} \psi(u,f) R_u(f), \tag{13}$$

where $R_u(f)$ is defined in Section III-B, with $f\in\mathcal{F}$. Since the aggregate access link rate of each flying base station (FBS) should not exceed the rate of the backhaul link, i.e., the link between FBS and the ground network infrastructure, the adjusted access link rate, denoted as $\widetilde{R}_u^{\rm ac}$ for user $u\in\mathcal{U}$, can be given as

$$\widetilde{R}_u^{\rm ac} = \underbrace{\min\left(\sum_{v\in\mathcal{U}_{i(u)}} R_v^{\rm ac}, R^{\rm bk}_{i(u)}\right)}_{\substack{Minimum\ of\ access\ and \\ backhaul\ link\ rates}} \underbrace{\frac{R_u^{\rm ac}}{\sum_{v\in\mathcal{U}_{i(u)}} R_v^{\rm ac}}}_{\substack{Proportional\ rate \\ allocation\ among\ users}} \tag{14}$$

where $R^{\rm bk}_{i(u)}$ is the backhaul link rate of user u's serving base station, i.e., $i(u)$ and $\mathcal{U}_{i(u)}$ is the set of users sharing the base station $i(u)$. In (14), the first item on the right-hand side is used to determine the minimum rate of the access and backhaul links, and the objective of the second item is to allocate the resulting minimum rate among the users sharing the same backhaul link.

D. Problem Statement

Finally, the control objective in FlyTera is to maximize the aggregate rate of all the users in $\mathcal{U}$, by jointly controlling the flight of the flying base stations in $\mathcal{B}_{\rm fly}$, their association with the ground users, as well as the spectrum band selection of the users, under the constraints of single-band access for the users and wireless backhual links for the flying base stations. Let $\mathbf{cod} = (\mathbf{cod}_i)_{i\in\widetilde{\mathcal{B}}}$ represent the coordinate vector of all the nodes in the network, and $\boldsymbol{\psi} = (\psi(u,f))_{u\in\mathcal{U}}^{f\in\mathcal{F}}$ denote the spectrum band selection vector of the users. Further denote $\boldsymbol{\zeta} = (\zeta_{ui})_{u\in\mathcal{U}}^{i\in\mathcal{B}}$ as the association vector, with $\zeta_{ui}=1$ if user u is associated with BS i and $\zeta_{ui}=0$ otherwise. If we consider single-home association for users, i.e., each user is allowed to be associated to at most one base station, then we have

$$\sum_{i\in\mathcal{B}} \zeta_{ui} \le 1,\ \forall u\in\mathcal{U}. \tag{15}$$

The FlyTera control problem can then be formalized as

$$\begin{array}{ll} Given: & \mathcal{U},\ \mathcal{B}_{\rm fly},\ \mathcal{B}_{\rm grd},\ \mathcal{F} \\ \underset{\mathbf{cod},\ \boldsymbol{\psi},\ \boldsymbol{\zeta}}{Maximize} & \sum_{u\in\mathcal{U}} \widetilde{R}_u^{\rm ac}(\mathbf{cod},\ \boldsymbol{\psi},\ \boldsymbol{\zeta}) \\ Subject\ to: & (1)-(15) \end{array} \tag{16}$$

where $\widetilde{R}_u^{\rm ac}(\mathbf{cod},\ \boldsymbol{\psi},\ \boldsymbol{\zeta}) = \widetilde{R}_u^{\rm ac}$ defined in (14) is the adjusted access link rate of user u.

The network control problem formulated in (16) is a mixed integer nonlinear nonconvex (MINLP) problem, because of the involved mathematical expression of $\widetilde{R}_u^{\rm ac}(\mathbf{cod},\ \boldsymbol{\psi},\ \boldsymbol{\zeta})$ and the binary association variables and frequency selection variables. Given an arbitrary such problem, it is still an open problem to obtain the global optimum solution with polynomial computational complexity. Recall in Section I that in this work our objective is to investigate the applicability of THz-band communications in mobile blockage-rich environments and how the THz band can complement the lower-frequency bands. To this end, in next section we solve problem (16) by designing distributed algorithms based on a combination of echo state learning and reinforcement learning, and then evaluate the performance of the algorithms in Section V.

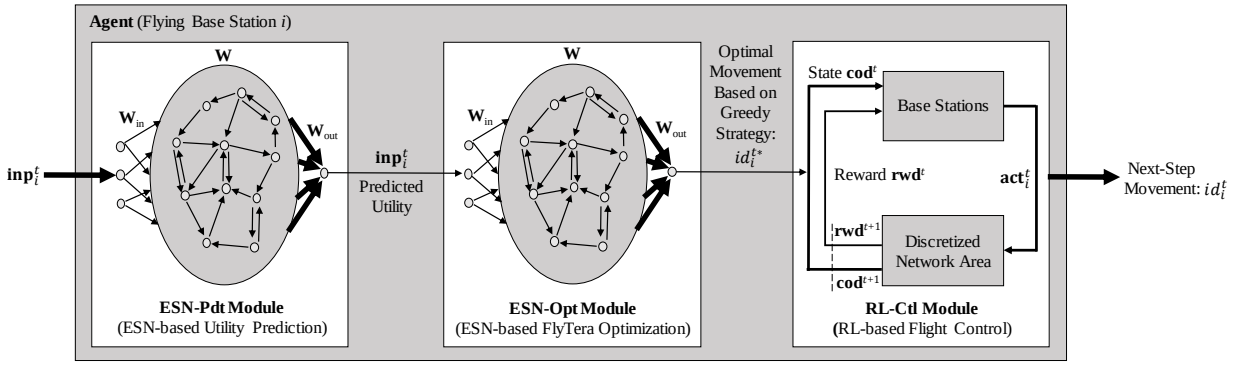

Fig. 3: Diagram of the distributed algorithm design based on a combination of echo state learning and reinforcement learning.

IV. Distributed Solution Algorithms

The framework of the distributed solution algorithm design is illustrated in Fig. 3, where there are three major modules, i.e., i) *ESN-based Utility Prediction (ESN-Pdt)*, ii) *ESN-based Utility Optimization (ESN-Opt)*, and iii) *RL-based FlyTera Control (RL-Ctl)*. The objective of *ESN-Pdt* is to predict the utility for each FBS by approximating the mapping from the network control variables, i.e., $\mathbf{cod}$, $\boldsymbol{\psi}$ and $\boldsymbol{\zeta}$ in (16), to the individual utility function $\widetilde{R}_u^{\mathrm{ac}}(\mathbf{cod},\ \boldsymbol{\psi},\ \boldsymbol{\zeta})$ based on echo state learning. Then, given the predicted utilities each FBS determines its own next-step action based on the *ESN-Opt* module. Finally, the *RL-Ctl* module is used to achieve a tradeoff between exploring and exploiting in favor of higher network spectral efficiency.

A. ESN-Pdt: ESN-based Utility Prediction

In FlyTera with distributed flying drone base stations, it is hard to obtain the complete and up-to-date network status information required for the base stations to derive the exact mathematical expression of $\widetilde{R}_u^{\mathrm{ac}}(\mathbf{cod},\ \boldsymbol{\psi},\ \boldsymbol{\zeta})$. To address this challenge, in this work we approximate the individual utility function $\widetilde{R}_u^{\mathrm{ac}}(\mathbf{cod},\ \boldsymbol{\psi},\ \boldsymbol{\zeta})$ based on echo state network (ESN). ESN is a new type of reservoir computing techniques for training recurrent neural networks [27]. Roughly speaking, as shown in Fig. 3, the objective of an ESN is to model approximately the mapping from the input signals to the output signals of a system, by training its input weights $\mathbf{W_{in}}$, the reservoir weights $\mathbf{W}$ and output weights $\mathbf{W_{out}}$ using a sigmoidal transfer function (e.g., hyperbolic tangent). Compared to traditional Neural Networks, which are computationally expensive, it is incredibly simple to train ESNs, while they are still able to model the complex time-varying behaviors of dynamical systems. Next we describe the *ESN-Pdt* module (the left block in Fig. 3) design in FlyTera.

The *ESN-Pdt* module consists of four components: *Agent*, *Input*, *Action* and *Reward Function*. In *ESN-Pdt*, the *Agent* refers to individual BSs in $\mathcal{B}_{\mathrm{fly}}$, i.e., each BS is endowed with an *ESN-Pdt* module for approximating its own utility function. Divide the time into a set of consecutive time slots $\mathcal{T}$. Then, in each time slot $t \in \mathcal{T}$, each BS $i \in \mathcal{B}_{\mathrm{fly}}$ feeds an *Input* (denoted as $\mathbf{inp}_i^t$) and a candidate *Action* (denoted as $\mathbf{act}_i^t$) to its *ESN-Pdt* module, which will then output the *Reward Function* value of the BS.

Input Design. The input of BS i's *ESN-Pdt* module in time slot t, defined as $\mathbf{inp}_i^t \triangleq \{\mathbf{cod}_{-i}^t,\ \boldsymbol{\psi}^t,\ \boldsymbol{\zeta}^t\}$, comprises of the locations of all the other BSs $\mathbf{cod}_{-i}^t = (\mathbf{cod}_j^t)_{j\in\mathcal{B}_{\mathrm{fly}}/i}$ with $\mathbf{cod}_j^t$ being the coordinate vector of BS j in time slot t, the association profile of the ground users $\boldsymbol{\zeta}^t$ as well as their spectrum band selection strategies $\boldsymbol{\psi}^t$ (confer Section III for the definitions of $\mathbf{cod}_j^t$, $\boldsymbol{\psi}^t$ and $\boldsymbol{\zeta}^t$)[1]. The dimension of $\mathbf{inp}_i^t$ increases quadratically with the scale of the network because of the association vector $\boldsymbol{\zeta}^t$. This can slow down the training of the *ESN-Pdt* module and hence degrade the utility approximation accuracy in large-scale networks. To address this challenge, we reform $\mathbf{inp}_i^t$ by reducing the number of primal variables in the input vector based on the following three simple but effective policies:

- *Policy 1: Shortest-Distance-Based Association*. Based on this policy, each ground user $u \in \mathcal{U}$ is associated to its nearest base station, i.e., the serving base station $i(u)$ is selected so that

$$i(u) = \arg\min_{i'\in\mathcal{B}_{\mathrm{fly}}} d_{i'u}(\mathbf{cod}_{i'},\ \mathbf{cod}_u),\ \forall u \in \mathcal{U}, \qquad (17)$$

  where $d_{i'u}(\cdot,\cdot)$ calculates the distance between two nodes as defined in (3).
- *Policy 2: Threshold-based Spectrum Selection*. Two distance thresholds are adopted, denoted as d_0^{mc} and d_0^{tz} with $d_0^{\mathrm{tz}} < d_0^{\mathrm{mc}}$, for the microwave and THz bands, respectively. Then, the microwave band will be selected for user u if $d_{u,i(u)}$, i.e., the distance between user u and its serving base station $i(u)$ determined based on Policy 1, satisfies $d_{u,i(u)} \geq d_0^{\mathrm{mc}}$; if $d_{u,i(u)} \leq d_0^{\mathrm{tz}}$, the THz band will be selected; otherwise, user u will use the mmWave band if $d_0^{\mathrm{tz}} < d_{u,i(u)} < d_0^{\mathrm{mc}}$.
- *Policy 3: Network Area Discretization*. The network area is divided into a number $N_x \times N_y \times N_z$ of three-dimensional rectangles, each with $\frac{L_x}{N_x}$, $\frac{L_y}{N_y}$ and $\frac{L_z}{N_z}$ for width, length and height, respectively. Denote $\mathcal{N}$ as the set of the resulting rectangles. Each rectangle $n \in \mathcal{N}$ is represented using a vector $\mathbf{rect}_n = (\widetilde{\mathbf{cod}}_n, id_n)$, where

[1] In previous sections, superscript t has been omitted in notations for the sake of convenience.

$\widetilde{\mathbf{cod}}_n$ is the coordinate vector of the center point of rectangle $n \in \mathcal{N}$, and $id_n = 0, 1, \cdots, N_x \times N_y \times N_z - 1$ is the index of the rectangle.

Based on Policies 1 and 2, the association and spectrum band selection vectors (i.e., $\boldsymbol{\psi}^t$ and $\boldsymbol{\zeta}^t$}) can be determined given the coordinates of all the BSs (i.e., $\mathbf{cod}^t$) in each time slot t. As a result, $\mathbf{cod}^t_{-i}$ becomes the only primal variable in $\mathbf{inp}^t_i$. The dimension of $\mathbf{inp}^t_i$ can be further reduced based on Policy 3 by mapping each component of $\mathbf{cod}^t_{-i}$ to the index of the corresponding rectangle. Finally, the input of the *ESN-Pdt* module can be rewritten as $\mathbf{inp}^t_i = (id^t_j)_{j \in \mathcal{B}_{\text{fly}}/i}$, with id^t_j being the index of BS j's rectangle in time slot t.

Action and Reward. Given input $\mathbf{inp}^t_i$ for the *ESN-Pdt* module for BS i in time slot t, BS i makes its action decisions and observes an output of the action. To this end, BS i chooses to move to a new rectangle in $\mathcal{N}$ except those occupied by other BSs. Hence, the set of actions for BS i, denoted as $\mathbf{act}^t_i$ for time slot t, can be written as

$$\mathbf{act}^t_i = \{id_m | m \in \mathcal{N}/\{n^t(j),\ j \in \mathcal{B}_{\text{fly}}/i\}\}, \tag{18}$$

where $n^t(j)$ represents the rectangle index of BS j in time slot t. The corresponding reward, denoted as $rwd^t_i(id_m)$, is determined by the aggregate rate achievable by the users it serves at new location id_m, i.e.,

$$rwd^t_i(id_m) = \sum_{v \in \mathcal{U}_i(id_m)} \widetilde{R}^{\text{ac}}_v, \tag{19}$$

where $\widetilde{R}^{\text{ac}}_v$ defined in (14) is the adjusted access rate of user v and $\mathcal{U}_i(id_m)$ is the set of users served by BS i at rectangle id_m.

B. ESN-Opt: ESN-based FlyTera Optimization

The job of the *ESN-Opt* module (the middle block in Fig. 3) is to determine the optimal next-step location for each BS, given the locations of all the other BSs. The agents and inputs of this module is the same as in *ESN-Pdt*, that is, *ESN-Opt* is also operated in individual flying BSs, and each BS takes the location information of the other BSs (i.e., $\mathbf{inp}^t_i$ defined above) as its input. Differently, the action set of BS i, denoted $\widetilde{\mathbf{act}}^t_i$ contains only single rectangle in each time slot t (its current rectangle), i.e., $\widetilde{\mathbf{act}}^t_i = \{id^t_i\}$. The reward, denoted as $\widetilde{rwd}^t_i$, is the maximum utility that BS i may achieve by moving to a new rectangle in next time slot, i.e.,

$$\widetilde{rwd}^t_i = \max_{id \in \mathbf{act}^t_i} rwd^t_i(id) \tag{20}$$

where rwd^t_i and $\mathbf{act}^t_i$ are the reward and the action set of BS i's *ESN-Pdt* module discussed in Section IV-A. Denote the resulting optimal next-step rectangle for BS i as id^{t*}_i.

C. RL-Ctl: Reinforcement Learning Based Flight Control

Based on a combination of the *ESN-Pdt* and *ESN-Opt* modules discussed above, each FBS determines its own best location for the next time slot. This may lead to a local optimum of the FlyTera control problem (16), which is not desirable. In favor of high network spectral efficiency, in this work we use reinforcement learning to guide the *exploration* and *exploitation* in the flight control of the BSs. Reinforcement learning (RL) [28] has been widely used to solve very complex problems that cannot be solved by conventional techniques. A RL consists of an environment and a set of agent states of the environment. The same as above discussed ESN modules, as shown in Fig. 3 (the right block), the RL agents are also the flying base stations, the environment is the discretized network area. The state of each agent i is denoted as $\mathbf{cod}^t_i$ in time slot t, and the feedback reward from the environment is denoted as $\mathbf{rwd}^t_i$. Then for any action $\mathbf{act}^t_i$ taken by the agent, let $\mathbf{cod}^{t+1}_i$ and $\mathbf{rwd}^{t+1}_i$ denote the corresponding state and reward at time $t+1$. The output of the *RL-Ctl* module is the next optimal action denoted as $\mathbf{act}^{t*}_i$ for the agent i in time slot t. In this paper, we design the *RL-Ctl* module based on ϵ-greedy exploration strategy [28].

Theorem 1. *If mixed strategies are adopted by the FBSs, the distributed algorithm proposed in this section converges to a stationary network operating point at which no FBS has incentive to fly to other locations if the other FBSs do not.*

Proof. Given the finite set of actions $\mathbf{act}^t_i$ defined in (18), let $\Delta(\mathbf{act}^t_i)$ represent the set of all probability distributions over the elements of $\mathbf{act}^t_i$, and $\boldsymbol{\pi}_i = [\pi_i(id_1), \cdots, \pi_i(id_{|\mathcal{N}|})]$ with $\boldsymbol{\pi}_i \in \Delta(\mathbf{act}^t_i)$ denoting the probability distribution used by BS $i \in \mathcal{B}$ to select an action from its action set $\mathbf{act}^t_i$, and $|\mathcal{N}|$ being the cardinality of the set of rectangles defined in Section IV-A. Then, the mixed strategy profile for BS i, denoted as $\boldsymbol{\pi}^*_i \in \Delta(\mathbf{act}^t_i), \forall\ i \in \mathcal{B}$, can be given as $\boldsymbol{\pi}^*_i = [\pi^*_i(id_1), \cdots, \pi^*_i(id_{|\mathcal{N}|})]$. The flight control and spectrum access problem (16) can then be reformulated as a non-cooperative game, and to prove this theorem it is sufficient to show that the game converges to a mixed Nash Equilibrium (NE) with mixed strategy probability [29]. Details of the proof are omitted due to limit of space. ■

V. Performance Evaluation

In this section, we first verify the effectiveness of the distributed solution algorithms proposed in Section IV and then analyze the performance of FlyTera. As of today, there are still no publicly available testbed or simulator that can support experiments of integrated aerial-ground wireless networking in the microwave, mmWave and THz spectrum bands. In this work we conduct simulations over a newly designed simulator called *SimBAG*.

A. SimBAG Design

SimBAG is a Python-based event-driven simulator for broadband integrated aerial-ground wireless networks. SimBAG comprises of four modules: *Network Configuration Module (NCM)*, *Network Element Module (NEM)*, *Discrete Event Driver (DED)*, and *Custom Algorithm Module (CAM)*. Through the NCM module, one can configure various network parameters, including the number of BSs and users, the bandwidth of each spectrum band, the transmission power of

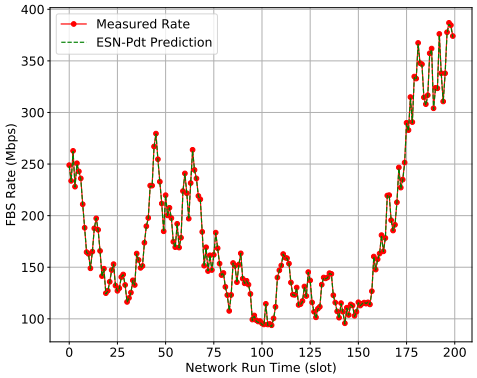

Fig. 4: Accuracy of rate prediction based on the *ESN-Pdt* module.

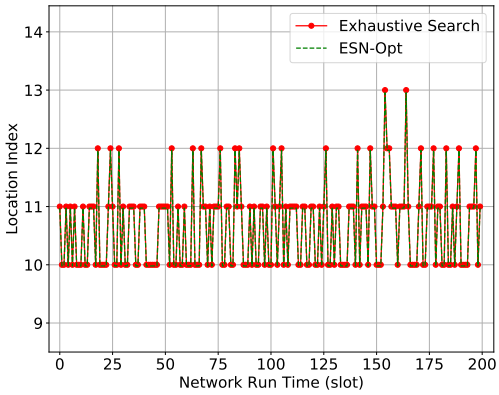

Fig. 5: Prediction accuracy of the optimal FBS movement based on the *ESN-Opt* module.

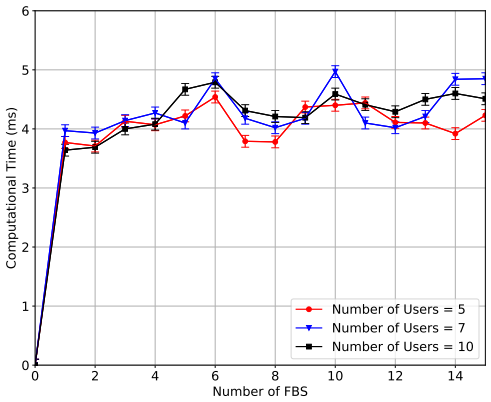

Fig. 6: Computational complexity of the *ESN-Opt* module.

the nodes, the simulation time, among others. Experimenters can also specify the pattern following which the blockages are generated and the drone base stations are deployed, e.g., Poisson Point Process and uniform distribution. The NEM module defines the classes for all the network elements, including Network, Ground Base Station, Flying Base Station, Blockage, Links, Interference, among others. These classes have been designed in a hierarchical manner. At the highest level is a general network element class net_elmt, which defines the basic network element attributes and operations such as registering an element in the network, specifying the parent and children elements of an element. The DED module provides the discrete network simulation environment based on the open-source library SimPy [30]. Finally, the CAM module hosts the custom-designed network control algorithms, e.g., the *ENS-Pdt* and *ESN-Opt* algorithms discussed in Section IV. APIs have been provided for all the four modules. The source code of the SimBAG project has been released to the community via GitHub [31].

B. Results and Discussion

Based on SimBAG a FlyTera network has been created with parameters configured through SimBAG's NCM module. We consider a network area of $200 \times 200 \times 50$ m^3. The center frequency is set to 3 GHz, 30 GHz and 300 GHz, and the bandwidth is set to 2 MHz, 40 MHz and 10 GHz for the microwave, mmWave and THz bands, respectively. The transmission power of BSs is set to 1 W, 250 mW and 20mW for the three bands. The number of BSs varies from 1 to 15 and the same for the users. The threshold distances d_0^{mc} and d_0^{tz} are set as 100 m and 10 m, respectively. The results are averaged over 50 simulations. Next we first evaluate the accuracy and complexity of the echo state learning algorithm, and then analyze the throughput achievable with different spectrum bands.

Accuracy and Complexity. In Figs. 4 and 5 we plot the accuracy of *ESN-Pdt* and *ESN-Opt*, by considering FlyTera with one base station and 10 users. The input and output weights of the *ESN-Pdt* and *ESN-Opt* in Fig. 3, i.e., $\mathbf{W}_{\text{in}}$ and $\mathbf{W}_{\text{out}}$, are initialized randomly. The reservoir weights $\mathbf{W}$ are initialized satisfying the Echo State Property (ESP) [27], which makes sure that the effect of the initial conditions vanishes after some time. In Fig. 4, the training data is collected in a total number of 10000 time slots, and the link rate is measured by moving the FBSs to random rectangles in each time slot. The accuracy of the trained *ESN-Pdt* module is tested in 200 more time slots. It can be seen that *ESN-Pdt* is able to predict the rate for FBSs with very high accuracy (98%) in all the tested time slots. Similarly, high accuracy (99%) can also be achieved by the *ESN-Opt* module in Fig. 5, where 9800 time slots have been used for training and 200 for testing. Here, the optimal next-step optimal location index is obtained by exhaustively searching all the rectangles of the network for each FBS. It is worth mentioning that exhaustive search is only needed at the training phase of the *ESN-Opt* module.

The computational complexity of the ESN learning is reported in Fig. 6, taking *ESN-Opt* as an example while similar results can be observed for *ESN-Pdt*. The experiments are conducted on a workstation with Intel(R) Core(TM) $i7-7700K$ CPU @ 4.20 GHz, memory of 32.0 GB, and 64-bit Windows Operating System. It can be seen that the prediction can be finished in less than 5 ms with different number of users and FBSs. For example, when the number of FBSs varies from 6 to 14, the average computational time is 4.4 ms, 5.0 ms and 4.2 ms for 5, 7, and 10 users, respectively. Therefore, based on echo state learning each FBS is able to predict its optimal movement in each time slot with very low and nearly constant computational complexity in different network settings.

Performance Analysis. In this experiment we analyze the

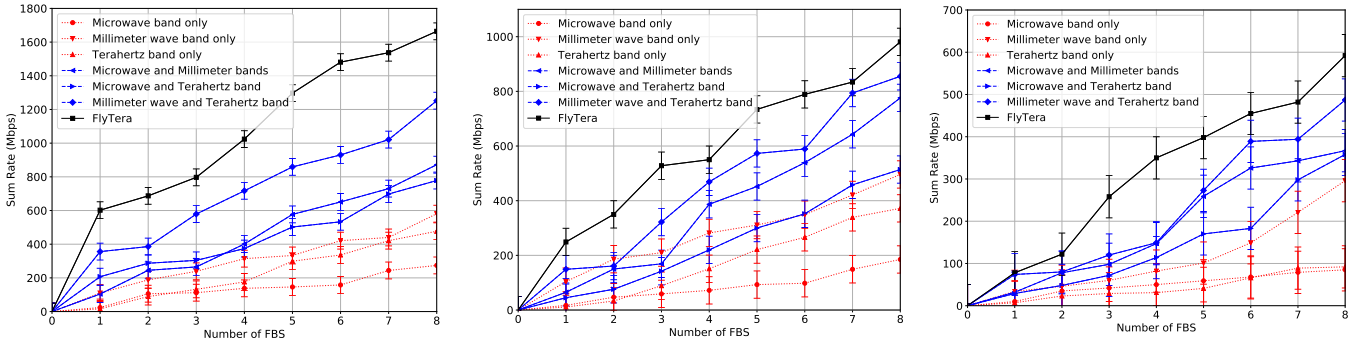

(a) (b) (c)

Fig. 8: Sum Rate of Network (a) Mobile FBS, (b) Static FBS with mobile users, and (c) Static FBS with Static users.

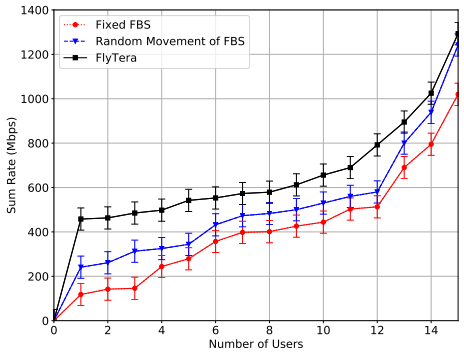

Fig. 7: Sum rate of the network with different number of users.

sum rate performance of the distributed control algorithms proposed in Section IV. We first consider one FBS and the number of users varying from 1 to 15 with step of 2. FlyTera is compared to two benchmark algorithms with fixed BS and randomly moving BS, respectively. The results are reported in Fig. 7. We found that the network sum rate can be significantly increased by FlyTera, with average gain of 24% and 40% comparing to random movement and fixed FBS. For example, in the case of 2 users a sum rate of 463 Mbps can be achieved by FlyTera, which is 261 Mbps and 142 Mbps for random movement and fixed FBS, respectively. This experiment proves the superiority of the FlyTera control algorithm.

In the following experiments, FlyTera is evaluated in three different scenarios: i) mobile FBS, ii) static FBS with mobile users, and iii) static FBS with static users. In each scenario, FlyTera is compared with six benchmark spectrum access schemes: i) microwave band only, (ii) mmWave band only, iii) THz band only, iv) microwave and mmWave bands, v) microwave and THz bands, and vi) mmWave and THz bands. The results are plotted in Fig. 8. As expected, in all scenarios the sum rate increases with the number FBSs but at different speeds. For example, in Fig. 8(a) the sum rate increases by 24 Mbps on average by deploying one more FBS in the microwave band, which are 56 Mbps and 52 Mbps for the mmWave and THz bands, respectively. The corresponding network spectral efficiency gain are 16 bps/Hz/FBS, 2 bps/Hz/FBS and 3×10^{-3} bps/Hz/FBS for the microwave, mmWave and THz bands, respectively. Therefore, although the available bandwidth is much wider, e.g., 10 GHz for THz vs 2 MHz for microwave in this experiment, both the mmWave and THz bands cannot be used alone to achieve orders of magnitude higher network capacity than that of the microwave band, primarily because of the significantly lower spectral efficiency.

From these experiments we also find that, which is a bit surprising, obviously *higher rather than lower* sum rate can be achieved by the THz band in mobile than in static environments. For example, the sum rate is around 500 Mbps and 370 Mbps with 8 mobile FBSs in Figs. 8(a) and 8(b), respectively, while it is only less than 100 Mbps in Fig. 8(c) where both FBSs and users are static. This is without no reasons. While a single THz link can be easily disconnected in blockage-rich environments, the problem can be effectively mitigated in FlyTera by adaptively deploying the flying base stations so that line-of-sight links can be maintained in most time. Therefore, it is paramount to exploit the mobility gain in future wireless networks in the THz band.

Finally, We find that FlyTera achieves the highest sum rate in all the three tested scenarios, which is 6, 5, and 7 times higher than that using the microwave band only. Particularly, in Fig. 8(a) obviously higher sum rate can be achieved with mobile FBSs than simply adding up the rates of the three single-band cases. For example, in the case of 8 FBSs, the sum rate is around 1650 Mbps for FlyTera, while 274 Mbps, 581 Mbps and 477 Mbps for the microwave, mmWave and THz bands with the corresponding sum rate of 1332 Mbps. Similar results can also be observed for the cases using two spectrum bands in Figs. 8(b) and (c). This verifies the effectiveness and importance of joint flight and spectrum access control in FlyTera.

In Fig. 9 we show the fairness results considering mobile and static FBSs and different spectrum access strategies similar to Fig. 8. We use Jain's Fairness Index as the measure of the rate allocation fairness. We can see that, in the case of microwave band only, the network achieves the best fairness (0.98), while the data rates of the users are the lowest (Fig. 8). Similarly, when we consider millimeter or terahertz band only, the fairness indices are 0.6 and 0.7 in the case of mobile scenario and only 0.4 and 0.5 in static scenario. The same trend can be observed for the combinations of frequency bands as well. Finally, we can see that with FlyTera the network

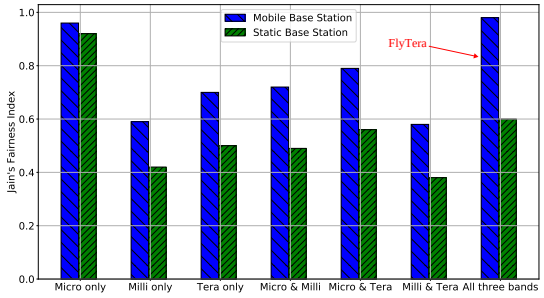

Fig. 9: Rate Allocation Fairness.

achieves a fairness index almost the same as that of the microwave band in mobile scenario, while still achieving the highest user rate (Fig. 8). This verifies the capability of FlyTera in achieving a good tradeoff between higher network spectral efficiency and better network coverage.

VI. Conclusions

In this paper, we have studied the problem of joint flight control and spectrum access in mobile blockage-rich environments in the microwave, mmWave and THz bands. We first provided a mathematical formulation of the FlyTera control problem, which is shown to be a MINLP problem. Then we designed distributed solution algorithms based on a combination of echo state learning and reinforcement learning theories. An event-driven simulator called SimBAG has been developed, over which the effectiveness and efficiency of the algorithms are verified and the performance of FlyTera is analyzed through an extensive simulation campaign. It is found that the THz-band wireless networks can significantly benefit from the mobility of FBSs and users in blockage-rich environments.

References

[1] E. Baştuğ, M. Bennis, M. Médard, and M. Debbah, "Toward Interconnected Virtual Reality: Opportunities, Challenges, and Enablers," *IEEE Communications Magazine*, vol. 55, no. 6, pp. 110–117, June 2017.

[2] G. A. Siles, J. M. Riera, and P. G. del Pino, "Atmospheric Attenuation in Wireless Communication Systems at Millimeter and THz Frequencies [Wireless Corner]," *IEEE Antennas and Propagation Magazine*, vol. 57, no. 1, pp. 48–61, Feb 2015.

[3] C. Han, A. O. Bicen, and I. F. Akyildiz, "Multi-Wideband Waveform Design for Distance-Adaptive Wireless Communications in the Terahertz Band," *IEEE Transactions on Signal Processing*, vol. 64, no. 4, pp. 910–922, Feb. 2016.

[4] C. Han and I. F. Akyildiz, "Distance-Aware Bandwidth-Adaptive Resource Allocation for Wireless Systems in the Terahertz Band," *IEEE Transactions on Terahertz Science and Technology*, vol. 6, no. 4, pp. 541–553, July 2016.

[5] I. F. Akyildiz and J. M. Jornet, "Realizing Ultra-Massive MIMO (1024x1024) Communication in the (0.06–10) Terahertz Band," *Nano Commun. Networks J., Elsevier*, vol. 8, pp. 46–54, 2016.

[6] H. Hassanieh, O. Abari, M. Rodriguez, M. Abdelghany, D. Katabi, and P. Indyk, "Fast Millimeter Wave Beam Alignment," in *Proc. of Conference of the ACM Special Interest Group on Data Communication*, Budapest, Hungary, August 2018.

[7] M. Hashemi, A. Sabharwal, C. E. Koksal, and N. B. Shroff, "Efficient Beam Alignment in Millimeter Wave Systems Using Contextual Bandits," in *Proc. of IEEE ICC*, Honolulu, HI, April 2018.

[8] S. Sur, X. Zhang, P. Ramanathan, and R. Chandra, "BeamSpy: Enabling Robust 60 GHz Links Under Blockage," in *Proc. of NSDI*, Santa Clara, CA, March 2016.

[9] A. Alkhateeb, I. Beltagy, and S. Alex, "Machine learning for reliable mmWave systems: Blockage prediction and proactive handoff," in *Proc. of IEEE Global Conference on Signal and Information Processing (GlobalSIP)*, Anaheim, CA, Nov. 2018.

[10] I. F. Akyildiz, C. Han, and S. Nie, "Combating the Distance Problem in the Millimeter Wave and Terahertz Frequency Bands," *IEEE Communications Magazine*, vol. 56, no. 6, pp. 102–108, June 2018.

[11] X. Wang, L. Kong, F. Kong, F. Qiu, M. Xia, S. Arnon, and G. Chen, "Millimeter Wave Communication: A Comprehensive Survey," *IEEE Communications Surveys Tutorials*, vol. 20, no. 3, pp. 1616–1653, thirdquarter 2018.

[12] R. Kovalchukov, D. Moltchanov, A. Samuylov, A. Ometov, S. Andreev, Y. Koucheryavy, and K. Samouylov, "Analyzing Effects of Directionality and Random Heights in Drone-Based mmWave Communication," *IEEE Transactions on Vehicular Technology*, vol. 67, no. 10, pp. 10 064–10 069, October 2018.

[13] G. Yang, Y. Zhang, Z. He, J. Wen, Z. Ji, and Y. Li, "Machine-learning-based prediction methods for path loss and delay spread in air-to-ground millimetre-wave channels," *IET Microwaves, Antennas Propagation*, vol. 13, no. 8, pp. 1113–1121, 2019.

[14] W. Yi, Y. Liu, M. Elkashlan, and A. Nallanathan, "Modeling and Coverage Analysis of Downlink UAV Networks with MmWave Communications," in *Proc. of IEEE International Conference on Communications Workshops (ICC Workshops)*, Shanghai, China, May 2019.

[15] L. Zhu, J. Zhang, Z. Xiao, X. Cao, D. O. Wu, and X. Xia, "3-D Beamforming for Flexible Coverage in Millimeter-Wave UAV Communications," *IEEE Wireless Communications Letters*, vol. 8, no. 3, pp. 837–840, June 2019.

[16] M. Gapeyenko, V. Petrov, D. Moltchanov, S. Andreev, N. Himayat, and Y. Koucheryavy, "Flexible and Reliable UAV-Assisted Backhaul Operation in 5G mmWave Cellular Networks," *IEEE Journal on Selected Areas in Communications*, vol. 36, no. 11, pp. 2486–2496, Nov 2018.

[17] Y. Ke, H. Gao, W. Xu, L. Li, L. Guo, and Z. Feng, "Position Prediction Based Fast Beam Tracking Scheme for Multi-User UAV-mmWave Communications," in *Proc. of IEEE ICC*, Shanghai, China, May 2019.

[18] Z. Xiao, P. Xia, and X. Xia, "Enabling UAV cellular with millimeter-wave communication: potentials and approaches," *IEEE Communications Magazine*, vol. 54, no. 5, pp. 66–73, May 2016.

[19] Z. Khosravi, M. Gerasimenko, S. Andreev, and Y. Koucheryavy, "Performance Evaluation of UAV-Assisted mmWave Operation in Mobility-Enabled Urban Deployments," in *Proc. of Int'l Conference on Telecommunications and Signal Processing (TSP)*, Athens, Greece, July 2018.

[20] Z. Feng, L. Ji, Q. Zhang, and W. Li, "Spectrum Management for MmWave Enabled UAV Swarm Networks: Challenges and Opportunities," *IEEE Commun. Magazine*, vol. 57, no. 1, pp. 146–153, Jan 2019.

[21] M. Chen, W. Saad, and C. Yin, "Echo State Learning for Wireless Virtual Reality Resource Allocation in UAV-Enabled LTE-U Networks," in *Proc. of IEEE ICC*, Kansas City, MO, May 2018.

[22] L. Zhang, H. Zhao, S. Hou, Z. Zhao, H. Xu, X. Wu, Q. Wu, and R. Zhang, "A Survey on 5G Millimeter Wave Communications for UAV-Assisted Wireless Networks," *IEEE Access*, vol. 7, pp. 117 460–117 504, 2019.

[23] J. M. Jornet and I. F. Akyildiz, "Channel Modeling and Capacity Analysis for Electromagnetic Wireless Nanonetworks in the Terahertz Band," *IEEE Transactions on Wireless Communications*, vol. 10, no. 10, pp. 3211–3221, Oct 2011.

[24] K. Ntontin and C. Verikoukis, "Toward the Performance Enhancement of Microwave Cellular Networks Through THz Links," *IEEE Transactions on Vehicular Technology*, vol. 66, no. 7, pp. 5635–5646, July 2017.

[25] T. Bai, R. Vaze, and R. W. Heath, "Analysis of Blockage Effects on Urban Cellular Networks," *IEEE Transactions on Wireless Communications*, vol. 13, no. 9, pp. 5070–5083, Sept. 2014.

[26] S. Yi, Y. Pei, and S. Kalyanaraman, "On the Capacity Improvement of Ad Hoc Wireless Networks Using Directional Antennas," in *Proc. of ACM International Symposium on Mobile Ad Hoc Networking Computing*, Annapolis, Maryland, 2003.

[27] M. Lukoševičius, "A Practical Guide to Applying Echo State Networks," *Lecture Notes*, Jan. 2012.

[28] R. S. Sutton and A. G. Barto, "Reinforcement Learning: An Introduction." Cambridge, MA, USA: MIT Press, 1998.

[29] T. Basar and G. J. Olsder, *Dynamic Noncooperative Game Theory (Classics in Applied Mathematics)*. USA: Society for Industrial and Applied Mathematics, 1999.

[30] "Simpy." [Online]. Available: https://pypi.org/project/simpy/

[31] https://github.com/ubwingslab/new-spectrum-technology.